THE JOURNAL OF PHYSICAL CHEMISTRY B

ARTICLE

pubs.acs.org/JPCB

Spatial Diffusion of Water in Carbon Nanotubes: From Fickian to Ballistic Motion

A. Barati Farimani and N. R. Aluru*

Department of Mechanical Science and Engineering, Beckman Institute for Advanced Science and Technology, University of Illinois at Urbana−Champaign, Urbana, Illinois 61801, United States

ABSTRACT: We investigate the spatial variation of the axial, radial, and tangential diffusion coefficients in carbon nanotubes (CNTs) of various diameters. The effect of confinement and CNT wall on the diffusion coefficient is studied. On the basis of the spatial variation of the diffusion coefficient, the diffusion mechanisms in different regions of the nanotube are identified. The dependence of the diffusion coefficient on the carbon−water interaction parameter is investigated. The average diffusion coefficient in the nanotube as a function of the nanotube diameter is computed, and the diffusion mechanisms, including the transition regimes, are identified. The results are analyzed via hydrogen bonds and water orientations.

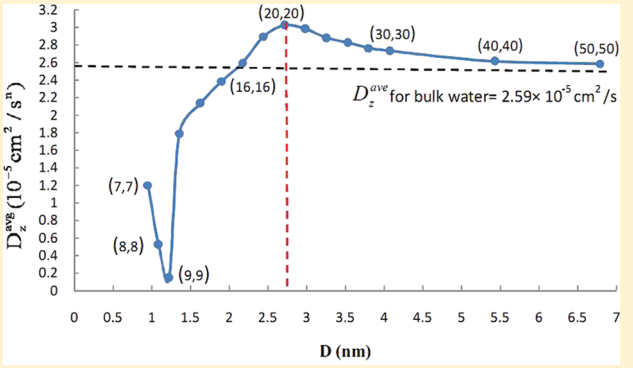

INTRODUCTION

Carbon nanotubes (CNTs) have recently been investigated extensively for various applications in nanofluidics including channels, sensors, filters, and gating devices.[1−3] Fluid transport in carbon nanotubes has been investigated for over a decade now.[4−7] Molecular dynamics (MD) simulations have been performed to understand different aspects of water transport in CNTs.[8−10] However, comparatively, there have been fewer experimental studies, and many of these studies have focused primarily on enhanced water transport in CNTs.[11,12] Confinement of water molecules in CNTs leads to several interesting properties.[13,14] CNTs with different diameters were studied to understand the thermodynamic driving force and phase transition of water.[15,16] Flow enhancement of water in CNTs, when compared to classical theories, has attracted the attention of researchers to find the underlying mechanism.[8] Among all the properties of water in confined CNTs, diffusion plays a key role and is important in defining other properties such as viscosity, permeability, flow type, and convection heat transfer.[9] A few studies were performed to develop a fundamental understanding of the diffusion mechanisms and diffusion enhancement of water inside CNTs.[17−21] Single-file diffusion (SFD) for small-diameter CNTs (diameter less than 1.4 nm) was investigated using NMR.[17,18] Striolo[19] reported that neither SFD nor ballistic diffusion may be observed if the simulation is performed for long enough time in narrow CNTs. The diffusion coefficient of water in different diameters of CNT was reported in ref 22, and different diffusion mechanisms were observed. The diffusion coefficient for zigzag and armchair CNT configurations was computed in refs 23 and 24. No prior studies were, however, performed to understand the spatial variation of the diffusion of water in CNTs and the effect of CNT surface on diffusion. In this paper, we compute the spatial variation of the diffusion coefficient of water in various diameter CNTs by paying particular attention to the diffusion of water near the CNT wall. The effect of confinement and surface contribution and their interplay is understood in detail by considering CNT diameters ranging from 0.95 to 6.8 nm. To investigate the spatial variation of the diffusion coefficient, the hydrogen bonding (HB) dynamics is computed. The connection between the HB network and diffusion enhancement near the CNT wall is elaborated and discussed. To understand the effect of confinement, radial, tangential, and axial diffusion coefficients are computed. To understand the effect of CNT surface on diffusion of water, we also consider smooth nanotubes with stronger carbon−oxygen interaction.

METHODS

Molecular dynamics simulations were performed using Gromacs 3.3.3.[25] A periodic boundary condition was applied in the axial direction (z). A schematic of the simulation setup is shown in Figure 1. Temperature was maintained at 300 K by applying the Nosé−Hoover thermostat with a time constant of 0.1 ps.[26,27] A simple point charge−extended (SPC/E) model was used for water.[9] Lennard-Jones parameters for the carbon atoms are σ = 0.339 nm and ε = 0.2897 kJ/mol.[28]The cutoff distance for the LJ interactions is 15 Å. The long-range electrostatic interactions were computed by using the particle mesh Ewald method (real space cutoff, 10 Å; reciprocal space gridding, 1.2 Å, fourth-order interpolation). Carbon atoms were frozen to their lattice position to prevent out-of-plane displacement. Molecular dynamics studies

Received: June 22, 2011
Revised: September 12, 2011
Published: September 13, 2011

dx.doi.org/10.1021/jp205877b | J. Phys. Chem. B 2011, 115, 12145–12149

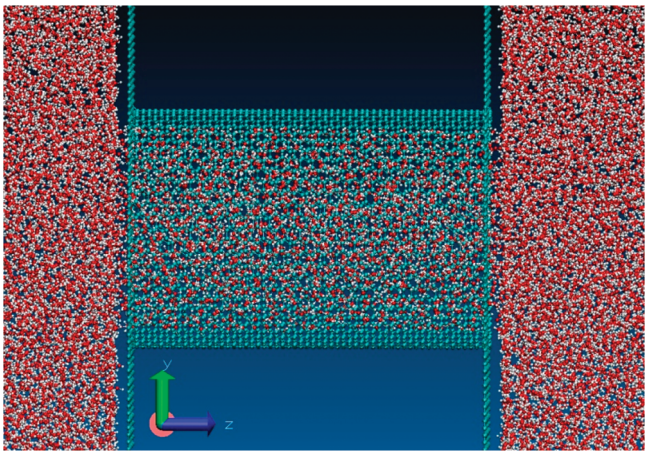

Figure 1. Schematic configuration of water simulation inside a CNT.

on nanofluidic properties of CNTs under equilibrium conditions have shown that treating CNTs as rigid in their lattice is a reasonable approximation.[29,30] The SETTLE algorithm was used to maintain the geometry of the water molecules. Initially, the system was equilibrated for 1 ns. The error bars in the results are the standard deviations based on four different initial configurations. The Parinello−Rahman scheme with a time constant of 0.1 ps and compressibility of 4.5×10^{-5} bar^{-1} was used to adjust the pressure of the system at 0.1 MPa.[9] In all cases, the equilibrium density of the bulk reservoir was around 1 g/cm^3. After equilibration, the simulation was run for an additional 6−10 ns. Time integration was performed by applying the leapfrog algorithm with a time step of 1.0 fs. Results for diffusion and hydrogen bonding were computed based on 300 ps intervals at a 50.0 fs sampling rate. To avoid entrance effects, only the middle part of the CNT was considered. Simulations contained 1700−18 000 water molecules depending on the size of the tube. All simulations were performed in the NVT ensemble. The diffusion coefficient is computed from the mean-squared displacement (MSD) of the water molecules' center of mass. The general formula to compute the diffusion coefficient is given by

$$\langle |(r(t) - r(0))|^2 \rangle = ADt^n \quad (1)$$

where r denotes the center of mass coordinate of the water molecule; the angle bracket defines the average over all the water molecules; t is the time interval; D is the diffusion coefficient; A is the dimensional factor which takes values of 2, 4, and 6 for 1-, 2-, and 3-dimensional diffusion, respectively; and n defines the type of the diffusion mechanism. To compute the average axial (z-direction) diffusion coefficient (denoted by D_z^{ave}), the MSD of all the molecules in that direction with $A = 2$ is used. A best linear fit to MSD gives the values of D_z^{ave} and n in eq 1. For the average diffusion coefficient (averaged over all three directions and denoted by D_{xyz}^{ave}) in the tube, the MSD of all the molecules in all the three directions with $A = 6$ is used (see Figure 1). Depending on how the MSD varies with time, different diffusion mechanisms can be identified; i.e., $n = 0.5$ refers to single-file diffusion, $n = 1$ refers to the Fickian diffusion, and $n = 2$ refers to ballistic diffusion.[19]

For bulk systems, MSD usually scales linearly with time ($n = 1$), and Fickian diffusion is observed. It should be noted that in eq 1 the slope of the MSD curve is computed at long time instances (20 ps < t < 40 ps), and t is quite large in comparison to the simulation time step. For bulk water, based on our computations, D_{xyz}^{ave} is 2.59×10^{-5} cm^2/s. This result is in good comparison with the results in ref 31. The experimental value of D_{xyz}^{ave} for bulk water is 2.3×10^{-5} cm^2/s, which is close to our computational value.[32]

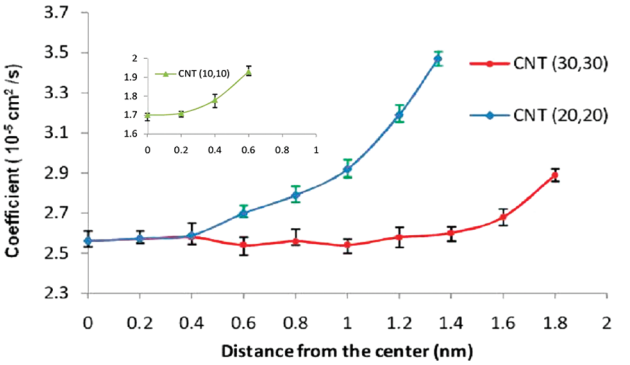

Figure 2. Spatial variation (from the center to the nanotube wall) of the diffusion coefficient along the axial direction (D_z^{Spat}) in (10,10) CNT (shown in inset), (20,20) CNT, and (30,30) CNT. (Note that the exponent of time (n) is not the same and varies with the distance from the center. This variation is shown in Figure 4.)

RESULTS AND DISCUSSION

Spatial Variation of the Axial Diffusion Coefficient. We computed the spatial variation of the axial diffusion coefficient, denoted by $D_z^{Spat}(A = 2)$, to understand how the diffusion coefficient varies from the tube center to the tube wall. Cylindrical bins are used to compute the spatial variation. The average diffusion coefficient in the axial direction is computed in each bin. The spatial variation of the axial diffusion coefficient in (10,10), (20,20), and (30,30) CNTs is shown in Figure 2. In both (20,20) and (30,30) CNTs, D_z^{Spat} is close to the bulk value (D_{bulk}^{avg} = 2.59×10^{-5} cm^2/s) in the center portion of the tube. Bulk diffusion behavior is observed up to distances of 0.4 and 1.2 nm from the center of the tube for (20,20) CNT and (30,30) CNT, respectively. Beyond these distances, the diffusion coefficient starts to increase, and an axial diffusion coefficient larger than the bulk value (diffusion enhancement) is observed near the walls of both CNTs. For (10,10) CNT, diffusion coefficient is lower than the bulk value in the central region of the tube, and a small enhancement is observed near the wall. Confinement effects reduce diffusion of water molecules in the central region of (10,10) CNT. Larger diameter nanotubes (e.g., (30,30) CNT) have a larger bulklike region compared to the smaller diameter nanotubes (e.g., (20,20) CNT). While diffusion enhancement is observed near the nanotube walls in both (20,20) and (30,30) CNTs, the variation is much sharper in the (20,20) CNT compared to that in the (30,30) CNT. From these results, we can conclude that the spatial variation of the axial diffusion coefficient depends on the size of the nanotube. As the diameter of the nanotube increases, more bulklike region is observed, and the effect of the surface diminishes.

To understand the effect of the surface on diffusion enhancement, we computed the spatial variation of the average number of hydrogen bonds (HB(n)) from the tube center to the surface of the CNT. Hydrogen bonding is defined by applying the geometric criteria where the acceptor−donor (O···O) distance is less than 0.35 nm and the angle (O−H···O) is less than 30°.[8] The average number of hydrogen bonds HB(n) was computed from the center to the surface of (30,30) and (20,20) CNTs, and

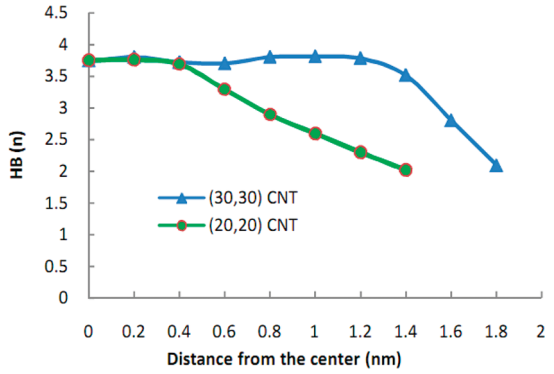

Figure 3. Spatial variation of the average number of hydrogen bonds (HB(n)) from the center to the surface of the CNT.

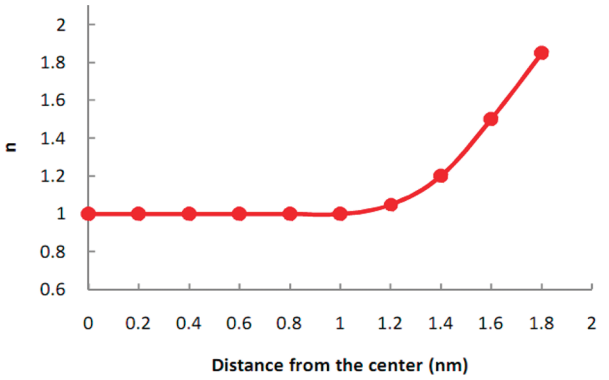

Figure 4. Spatial variation (from the tube center to the surface) of n for the (30,30) CNT. n defines the type of diffusion mechanism.

these results are shown in Figure 3. In the center of the tube, HB(n) is 3.7 which is equal to HB(n) for bulk water. As we approach the nanotube wall, HB(n) is reduced to about 2.1 in both (20,20) and (30,30) CNTs. Depletion of hydrogen bonds near the surface is due to the geometrical configuration, which prevents the hydrogen bonds to form. For example, free OH bonds are observed near the surface (because of geometrical constraints), and these bonds are not involved in hydrogen bonding.[8] These dangling OH bonds change the dynamics of molecules near the surface. The reduced number of hydrogen bonds provides more degrees of freedom for the water molecules which results in enhanced diffusion near the surface of the CNT. It should be noted that if the molecules with depleted number of hydrogen bonds cannot diffuse freely because of geometrical constraints then enhanced diffusion may not be observed. For example, in the (6,6) CNT, the average number of hydrogen bonds is about 1.71, and the diffusion in this case is quite small due to geometrical confinement.[9,16,29]

As mentioned in the Methods section, the diffusion mechanism is defined by the power (n) in eq 1. Figure 4 shows the spatial variation of n in the (30,30) CNT. In the center region of the nanotube, n = 1 signifying that the diffusion mechanism is Fickian. As shown in Figure 2 and Figure 3, and as discussed above, in the center region of the nanotube, HB(n) and D_z^{Spat} have bulk values since the molecules are fully hydrogen bonded and are not geometrically confined. The molecules move over each other with an average of 3.7 HBs. As we approach the surface of the nanotube, n > 1 is observed, suggesting non-Fickian diffusion. In particular, very close to the wall of the CNT, n is close to 2, implying that water molecules undergo ballistic diffusion. For distances larger than 1 nm from the center of the tube and less than the tube radius, 1 < n < 2 is observed, and this region is denoted as the transition region between Fickian and ballistic diffusion motions. In summary, for sufficiently larger diameter CNTs, multiple diffusion mechanisms, namely, Fickian diffusion, transition-to-ballistic diffusion, and ballistic diffusion, can be observed in the same nanotube. In smaller diameter CNTs, not all three diffusion mechanisms may be present in the same tube.

Average Axial Diffusion Coefficient. We now investigate the average axial diffusion coefficient, D_z^{ave}, in different size carbon nanotubes with diameters ranging from 0.95 to 6.8 nm (see the Methods section for calculation of D_z^{ave}). Figure 5 shows the variation of D_z^{ave} with the diameter (D) of the CNT. For CNTs with D < 2.2 nm, D_z^{ave} is lower than the bulk value. In the case of the (9,9) CNT, anomalous diffusion behavior with low mobility is observed because of the ice-like structure of water.[9] For CNTs with D < 2.2 nm, confinement plays a dominant role leading to a reduction in the diffusion coefficient. Molecules are confined by the CNT in such a way that they cannot diffuse back and forth freely. Even though the depletion of hydrogen bonds is observed in these CNTs, the geometrical confinement overweighs, thereby reducing the diffusion coefficient to less than the bulk value.

For CNTs with 2.3 nm < D < 6 nm, D_z^{ave} is higher than the bulk value and attains the maximum for D = 2.7 nm. For these CNTs, the enhancement in diffusion is due to the surface contribution to depletion of HBs and the existence of the bulk region for normal diffusion of molecules (see Figure 1). For D larger than 2.7 nm, D_z^{ave} decreases from its maximum value until the bulk value is reached (approximately) for a CNT diameter of 6.0 nm. For D > 6.0 nm, D_z^{ave} is close to the bulk diffusion coefficient. For 2.7 nm < D < 6 nm, as the CNT size grows, the surface contribution to diffusion enhancement becomes negligible in comparison to the increase in the central region where bulk diffusion is observed. It is important to note that a thin layer of high diffusivity is always present near the surface of the CNT. For CNT diameters between 2.3 and 6 nm, this thin layer is significant enough, compared to the bulk core in the central region, such that an overall enhancement in the average diffusion coefficient is observed.

We next identify the diffusion mechanism based on the average axial diffusion coefficient in the CNT. Figure 6 shows the variation of n, the exponent in eq 1 which defines the diffusion mechanism, as a function of the CNT diameter. For CNTs with D < 1.5 nm, n < 1 and the diffusion mechanism is non-Fickian. As mentioned above, in this case, the diffusion coefficient is lower than the bulk diffusion coefficient. For the (7,7) CNT, with n = 0.7, the diffusion mechanism is found to be a transition from single-file diffusion to Fickian diffusion. For the (8,8) CNT, with $n \approx 0.5$, single-file diffusion is observed. In the (9,9) CNT, because of the formation of an ice-like structure, the diffusion coefficient is significantly reduced, and restricted diffusion is observed (n = 0.32, and molecules quiver in their place). The anomalous diffusion behavior in (9,9) CNT is due to the formation of a chain-like structure of water molecules. Recent studies have shown that the entropy is quite low for (8,8) and (9,9) CNTs, and this is due to specific H-bonding structure.[15] For 1.6 nm < D < 2.3 nm and D > 4.0 nm, n = 1 and Fickian diffusion is observed (bulk-like behavior). For 2.4 nm < D < 4.0 nm, 1 < n < 1.2 is observed, implying transitional diffusion, and water has higher mobility compared to the bulk value. It is important to note that even though ballistic diffusion is observed near the surface of the CNT

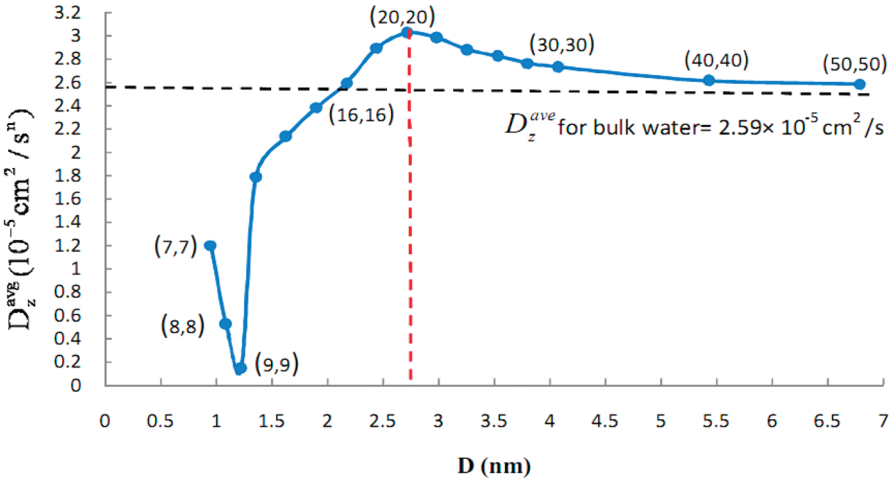

Figure 5. Variation of the average axial diffusion coefficient, D_z^{ave}, of water as a function of the diameter of the CNT. (Note that the exponent of time (n) is not the same for all the tubes, and the variation of n with the diameter is shown in Figure 6.)

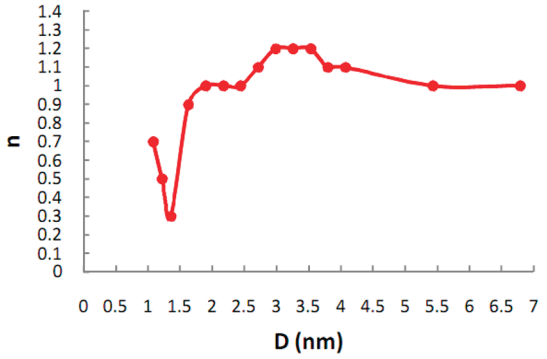

Figure 6. Variation of n, the exponent which defines the diffusion mechanism, as a function of the CNT diameter.

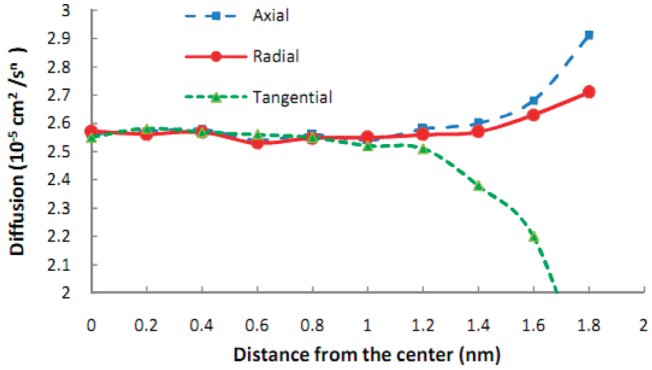

Figure 7. Spatial variation of the diffusion components ($D_{r,\theta,z}^{Spat}$) in the (30,30) CNT.

ballistic diffusion is not observed in the average axial diffusion coefficient, and only transition-to-ballistic diffusion is observed.

Diffusion in Cylindrical Coordinates. To understand, in more detail, the surface contribution of CNT to diffusion, we studied the spatial variation of diffusion in cylindrical coordinates ($D_{r,\theta,z}^{Spat}$) for the (30,30) CNT. In particular, the spatial variations of the radial (D_r^{Spat}), axial (D_z^{Spat}), and tangential diffusion (D_θ^{Spat}) are computed. Figure 7 shows the spatial variation of the diffusion components, D_r^{Spat}, D_θ^{Spat}, and D_z^{Spat}. Since the spatial variation of the axial diffusion coefficient, D_z^{Spat}, has already been discussed above, here we focus on the spatial variation of the radial and the tangential components.

Both the radial and the tangential diffusion components exhibit interesting behavior as the water molecules approach the surface of the CNT. The radial diffusion component increases (compared to the bulk value in the central region of the CNT) near the surface of the CNT, even though the increase/enhancement is not as significant as that of the axial diffusion component. The enhancement of the radial component near the surface could be due to (1) weaker carbon−water interaction compared to the water−water interaction ($(\varepsilon_{OW-OW})/(\varepsilon_{OW-C}) \approx 1.5$, ε is the LJ interaction energy); for water molecules within the cutoff distance from the CNT surface, this creates a momentum in the normal or the radial direction; (2) free OH bonds near the surface, which generally point toward the surface,[8] releasing energy due to the breaking of the hydrogen bonds.[33−35] This causes the water molecules to move along the directions where they are less confined (e.g., along the axial and normal directions, see Figure 3). The movement of water molecules in this layer (near the surface) is facilitated by having less hydrogen bonds.[33] The molecules diffuse back and forth in this layer, and there is a tendency to diffuse into the core region. Strong orientation effects near the hydrophobic surface[35] create lower entropy near the wall, and this causes the molecules to diffuse toward the core of the tube (higher entropy region). The tangential diffusion coefficient, D_θ^{Spat}, decreases near the CNT surface compared to the bulk value in the central region of the nanotube. Water movement in the tangential direction (θ) is hindered due to the surface curvature effect.

To further understand the effect of the carbon−water interaction potential, we changed the potential of CNT to fictitious silicon nanotubes (SiNT, this is analogous to a CNT with stronger carbon−oxygen interaction) as discussed in ref 8. Figure 8 shows the spatial variation of the three diffusion coefficients (in cylindrical coordinates), $D_{r,\theta,z}^{Spat}$, in SiNT. All the three components of diffusion, D_r^{Spat}, D_z^{Spat}, and D_θ^{Spat}, are reduced near the surface of the SiNT. This is because of the stronger interaction of the water molecules with the silicon atoms ($(\varepsilon_{OW-OW})/(\varepsilon_{OW-Si}) \approx 0.51$). The comparison between Figure 7 and Figure 8 reveals that the interatomic potential between water and the nanotube surface

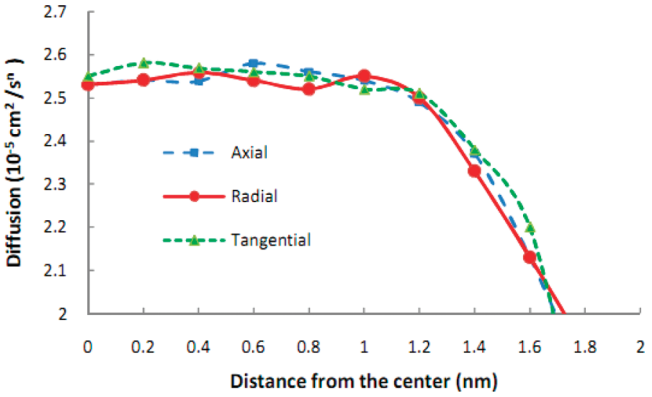

Figure 8. Spatial variation of the diffusion components ($D^{Spat}_{r,\theta,z}$) in the (30,30) SiNT.

(hydrophobic, hydrophilic, etc.) is critical in determining the diffusion of water near the surface. Previous studies have shown that the depletion of hydrogen bonds in SiNT is weaker compared to that in CNT.[8] As a result, diffusion is strongly reduced near the surface of the Si NT since silicon interacts strongly with water and the depletion of the HB network is not as strong as in the case of the CNT.

CONCLUSIONS

Spatial variation of the axial diffusion coefficient indicates that there is a significant enhancement of diffusion near the CNT wall. In larger diameter nanotubes, the diffusion mechanism is found to be Fickian in the central portion of the nanotube and ballistic near the nanotube wall. In smaller diameter naotubes, the diffusion coefficient is significantly reduced because of confinement. Diffusion enhancement near the CNT surface can be explained by the depletion of the hydrogen bonds, weak carbon−water interaction, and water orientation near the surface. The spatial variation of the radial and the tangential diffusion coefficients indicates that the radial diffusion coefficient is also enhanced near the surface while the tangential diffusion coefficient is reduced near the surface. The enhancement of the diffusion coefficient (axial and radial) near the surface depends strongly on the carbon−water interaction parameter. The average diffusion coefficient in the nanotube as a function of the CNT diameter indicates that the diffusion mechanism changes from "single-file" to "transition-to-normal" to "normal" to "transition-to-ballistic" to "normal" diffusion as the diameter increases.

AUTHOR INFORMATION

Corresponding Author

*E-mail: aluru@illinois.edu. Web: http://www.illinois.edu/∼aluru.

ACKNOWLEDGMENT

This research was supported by NSF under grants 0328162, 0810294, 0852657, and 0915718.

REFERENCES

(1) Lopez, C. F.; Nielsen, S. O.; Moore, P. B.; Klein, M. L. *Proc. Natl. Acad. Sci. U.S.A.* **2004**, *101*, 4431.
(2) Gao, Y.; Bando, Y. *Nature* **2002**, *415*, 599.
(3) Holt, J. K.; Noy, A.; Huser, T.; Eaglesham, D.; Bakajin, O. *Nano Lett.* **2004**, *4*, 2245.
(4) Hummer, G.; Rasaiah, J. C.; Noworyta, J. P. *Nature* **2001**, *414*, 188–190.
(5) Majumder, N.; Chopra, N.; Andrews, R.; Hinds, B. *Nature (London)* **2005**, *438*, 44.
(6) Brovchenko, I.; Geiger, A.; Oleinikova, A. *Phys. Chem. Chem. Phys.* **2001**, *3*, 1567.
(7) Whitby, M.; Quirke, N. *Nat. Nanotechnol.* **2007**, *2*, 87–94.
(8) Joseph, S.; Aluru, N. R. *Nano Lett.* **2008**, *8*, 452.
(9) Mashl, R. J.; Joseph, S.; Aluru, N. R.; Jakobsson, E. *Nano Lett.* **2003**, *3*, 589–592.
(10) Hanasaki, I.; Nakatani, A. *Nanotechnology* **2006**, *17*, 2794–2804.
(11) Hinds, B. J.; Chopra, N.; Rantell, T.; Andrews, R.; Gavalas, V.; Bachas, L. G. *Science* **2004**, *303*, 62–65.
(12) Holt, J. K.; Park, H. G.; Wang, Y.; Stadermann, M.; Artyukhin, A. B.; Grigoropoulos, C. P.; Noy, A.; Bakajin, O. *Science* **2006**, *312*, 1034–1037.
(13) Mukherjee, B.; Maiti, P. K.; Dasgupta, C.; Sood, A. K. *J. Nanosci. Nanotechnol.* **2007**, *7*, 1796–1799.
(14) Cicero, G.; Grossman, J. C.; Schwegler, E.; Gygi, F.; Galli, G. *J. Am. Chem. Soc.* **2008**, *130* (6), 1871–1878.
(15) Pascal, A. T.; Goddard, W. A.; Jung, Y. *Proc. Natl. Acad. Sci.* **2011**, *108* (29), 11794–11798.
(16) Srivastava, R.; Docherty, H.; Singh, J. K.; Cummings, P. T. *J. Phys. Chem. C* **2011**, *115*, 12448–12457.
(17) Mukherjee, B.; Maiti, P. K.; Dasgupta, C.; Sood, A. K. *ACS Nano* **2008**, *2* (6), 1189–1196.
(18) Das, A.; Jayanthi, S.; Deepak, H. S. M. V.; Ramanathan, K. V; Kumar, A.; Dasgupta, C.; Sood, A. K. *ACS Nano* **2010**, *4* (3), 1687–1695.
(19) Striolo, A. *Nano Lett.* **2006**, *6*, 633–639.
(20) Martí, J.; Gordillo, M. C. *Chem. Phys. Lett.* **2002**, *354*, 227.
(21) Allen, T. W.; Kuyucak, S.; Chung, S. H. *J. Chem. Phys.* **1999**, *111*, 7985.
(22) Alexiadis, A.; Kassinos, S. *Chem. Rev.* **2008**, *108* (12), 5014–5034.
(23) Won, C. Y.; Joseph, S.; Aluru, N. R. *J. Chem. Phys.* **2006**, *125*, 14701.
(24) Liu, Y. C.; Shen, J. W.; Gubbins, K. E.; Moore, J. D.; Wu, T.; Wang, Q. *Phys. Rev. B* **2008**, *77*, 125438.
(25) Van Der Spoel, D.; Lindahl, E.; Hess, B.; Groenhof, G.; Mark, A. E.; Berendsen, H. J. C. *J. Comput. Chem.* **2005**, *26*, 1701–1708.
(26) Nosé, S. *J. Chem. Phys.* **1984**, *81* (1), 511–519.
(27) Hoover, W. G. *Phys. Rev. A* **1985**, *31*, 1695–1697.
(28) Werder, T.; Walther, J. H.; Jaffe, R. L.; Halicioglu, T.; Koumoutsakos., P. *J. Phys. Chem. B* **2003**, *107* (6), 1345–1352.
(29) Kotsalis, E. M.; Walther, J. H.; Koumoutsakos, P. *Int. J. Multiphase Flow* **2004**, *30*, 995–1010.
(30) Hanasaki, I.; Nakatani, A. *J. Chem. Phys.* **2006**, *124*, 144708.
(31) Mark, P.; Nilsson, L. *J. Phys. Chem. A* **2001**, *105* (43), 9954–9960.
(32) Mills, R. *J. Phys. Chem.* **1973**, *77* (5), 685–688.
(33) Luzar, A.; Chandler, D. *Nature* **1996**, *379*, 55–57.
(34) Ricci, M. A.; Bruni., F; Gallo., P; Rovere, M.; Soper, A. K. *J. Phys.: Condens. Matter* **2000**, *12*, A345–A350.
(35) Scatena, L. F.; Brown, M. G.; Richmond, G. L. *Science* **2001**, *292*, 908–912.